International Institute for Applied Systems Analysis
IIASA www.iiasa.ac.at

Attainability Analysis of the DICE Model

Smirnov, A.

IIASA Interim Report
September 2005

International Institute for
Applied Systems Analysis
Schlossplatz 1
A-2361 Laxenburg, Austria

Tel: +43 2236 807 342
Fax: +43 2236 71313
E-mail: publications@iiasa.ac.at
Web: www.iiasa.ac.at

Interim Report **IR-05-049**

Attainability Analysis of the DICE Model

Alexey Smirnov (asmirnov@cs.msu.su)

Approved by

Arkady Kryazhimskiy (kryazhim@iiasa.ac.at)
Program Leader, Dynamic Systems

September 2005

Abstract

The paper is devoted to a development of a method for constructing attainability domains for the DICE model of the economic of global warming. Such domains allow one to observe all possible states of the model, to compare different strategies, and to perform sensitivity and uncertainty analysis. All this makes attainability domains an efficient tool for the evaluation of different strategies from the viewpoint of their rationality.

Key words: climate change, DICE model, attainability domains, sensitivity analysis, uncertainty analysis
JEL Classification: C6, Q5
Mathematics Subject Classification (2000): 37N40, 49K, 91B62, 93B03

About the Author

Alexey Smirnov
Department of Optimal Control
Faculty of Computational Mathematics & Cybernetics
Moscow State University, Leninskie Gory
Moscow 119992, Russia

Acknowledgments

This work was carried out within the Dynamic System Program as a part of the Young Scientists Summer Program at the International Institute of Applied Systems Analysis in 2004. The author is grateful to Arkady Kryazhimskiy (DYN) and Sergei Aseev (DYN) who initiated this research. It is also his pleasure to thank Brian O'Neil (POP) and Michael Obersteiner (FOR) for their attention, useful suggestions, and valuable comments.

Contents

Attainability Analysis of the DICE Model

Alexey Smirnov (asmirnov@cs.msu.su)

1 Introduction

Concepts and tools of the mathematical theory of optimal control are commonly used to analyze dynamical systems arising in natural and social sciences. Usually, optimal controls cannot be given explicitly and are found numerically. A common drawback of numerical solutions is their poor reliability; moreover, quite often numerical optimization algorithms find local solutions instead of the global ones, which leads to the necessity of more specific further analysis.

For a comprehensive numerical analysis of the model's dynamics, the control theory suggests another powerful tool: the attainability domains. The model's attainability domain at some (future) time t is understood as the set of all states that are potentially reachable by the model at time t. Generally, the attainability domain can be constructed without simulating a large number of the model's trajectories. Control-theoretic methods including the Pontryagin maximum principle [2], provide a fundamental basis for constructing efficient and error-robust approximations to the attainability domains (in particular, [4, 5] develop ellipsoidal approximations to the attainability domains for linear models).

The construction of the model's attainability domains can be viewed as a first step in the global analysis of the model's dynamics. A natural next step is drawing the optimal utility surface above the attainability domain. The hight of a point on the optimal utility surface depicts the maximum value of a utility function, achievable on the model's trajectories arriving at the underlying point in the attainability domain (for further details, see Section 7). The graphs of the attainability domains and the utility surfaces above them can be informative enough for making qualitative judgements on the global dynamical properties of the model.

In this paper we analyze the attainability domains and utility surfaces for the DICE model describing economic/climatic change. The original DICE model known today as DICE-94 was introduced by Nordhaus in [1]; its revised version, DICE-99, is described in [6]. Here, we state several qualitative properties of a modified DICE-94 model; in particular, we show that the model's utility surfaces are rather flat, and the model's states are rather insensitive to the CO_2 emission rate.

The paper is organized as follows. In Sections 2–3 we introduce the model's equations and parameters. In Section 4 we simplify the model. In Section 5 we compare the simplified model with the original one. In Section 6 we calibrate the model. In Section 7 we describe the attainability domains and utility surfaces. In Section 8 we carry out a detailed attainability analysis of the model. Section 9 is a summary.

2 DICE model

Our study is based on the DICE-94 model [1] (**D**ynamic **I**ntegrated model of **C**limate and the **E**economy) – a Ramsey type model of economic growth, complemented by climate equations. The model takes into account economic impacts of climate change and costs for emission reductions. The model's state variables include

$K(t)$, the world capital measured in trillion US dollars;
$M(t)$, the mass of greenhous gases in the atmosphere[1], measured in billion tons;
$T^U(t)$, the atmospheric temperature;
$T^L(t)$, the temperature of the deep ocean.

The model's decision (control) variables are

$s(t)$, the saving rate of capital;
$\mu(t)$, the CO_2 emission rate.

The total economic output $Q(t)$ (the gross world product, GWP) is described by the standard Cobb-Douglas production function of the technology stock $A(t)$, capital $K(t)$, and labor (population) $L(t)$:

$$Q(t) = \Omega(t)A(t)K(t)^{\gamma}L(t)^{1-\gamma}; \tag{1}$$

here γ is the elasticity of the economic output to capital, and $\Omega(t)$ relates the impact of emission reduction and climate change to the economic output. The functions $A(t)$ and $L(t)$ are defined exogenously.

The DICE equation describing the dynamics of the capital stock has the form

$$\frac{dK(t)}{dt} = s(t)Q(t) - \delta_K K(t), \tag{2}$$

here $s(t)Q(t)$ is the annual amount allocated for investment and δ_K is the capital deprecation rate. Owing to (1) and (2), we have

$$\frac{dK(t)}{dt} = s(t)\Omega(t)A(t)L(t)^{1-\gamma}K(t)^{\gamma} - \delta_K K(t). \tag{3}$$

The next equation describes the process of accumulation of GHGs in the atmosphere:

$$\frac{dM(t)}{dt} = \alpha E(t) - \delta_M(M(t) - \tilde{M}). \tag{4}$$

Here, $E(t)$ is the annual emission of GHGs (in CO_2-equivalent units), $\tilde{M}$ is the preindustrial amount of atmospheric carbon, α is the marginal atmospheric retention ratio, and δ_M is the rate of the deep ocean's uptake of atmospheric carbon. Equation (4) shows that the amount of atmospheric carbon (compared to that in the preindustrial period, $\tilde{M}$), grows due to emission and declines due to diffusion of carbon into the deep ocean.

Emission $E(t)$ is given by

$$E(t) = (1 - \mu(t))E_r(t). \tag{5}$$

Here, $E_r(t)$ is the CO_2 emission from industrial sources in the reference case assuming no special emission reduction efforts, and $\mu(t)$ characterizes the rate of emission reduction.

The non-controlled emission $E_r(t)$ is defined by

$$E_r(t) = \sigma(t)[A(t)L(t)^{1-\gamma}K(t)^{\gamma}] \tag{6}$$

where $[A(t)L(t)^{1-\gamma}K(t)^{\gamma}]$ is the economic output in the reference case (see (1)) and $\sigma(t)$ relating the total economic output to the industrial emission of CO_2 is given exogenously. Due to (4)–(6), we have

$$\frac{dM(t)}{dt} = \alpha(1-\mu(t))\sigma(t)A(t)L(t)^{1-\gamma}K(t)^{\gamma} - \delta_M(M(t)-\tilde{M}). \tag{7}$$

The accumulation of the GHGs leads to the increase of the temperature on the Earth surface through the increase of the radiative forcing. The latter is defined as a function of the amount of the accumulated GHGs (in CO_2 equivalent units):

$$F(t) = \eta \log_2\left(\frac{M(t)}{\tilde{M}}\right) + O(t); \tag{8}$$

here η is a forcing constant and $O(t)$ is the amount of the non-industrial GHGs.

Forcing $F(t)$ drives the dynamics of the atmospheric temperature $T^U(t)$:

$$\frac{dT^U(t)}{dt} = \frac{1}{R_1}\left(F(t) - \lambda T^U(t) - \frac{R_2}{\tau_{12}}\big(T^U(t)-T^L(t)\big)\right), \tag{9}$$

$$\frac{dT^L(t)}{dt} = \frac{1}{\tau_{12}}\big(T^U(t)-T^L(t)\big); \tag{10}$$

here $T^L(t)$ is the temperature of the deep ocean; R_1 is the thermal capacity of the upper layer of the ocean; R_2 is the thermal capacity of the deep ocean; τ_{12} is the rate of the top-down transfer of carbon in the ocean; and λ is a feedback parameter.

Factor $\Omega(t)$ (see (1)) reflecting the emission reduction cost and damage from global warming, links the economic part of the model, (3), to its climatic part, (7), (9), (10). As Nordhaus [1] suggests,

$$\Omega(t) = \frac{1-b_1\mu(t)^{b_2}}{1+\theta_1(T^U(t))^{\theta_2}}; \tag{11}$$

here b_1 and b_2 are mitigation cost parameters and θ_1 and θ_2 are damage parameters. Relation (11) shows that the total economic output is negatively related to both the global temperature and emission reduction effort.

The DICE model is formulated as an optimal control problem (see [2]). Namely it is assumed that the trajectories of the state variables ($K(t)$, $M(t)$, and others) are driven by specific time-varying controls $s(t)$ and $\mu(t)$ chosen so that social welfare, W, the utility index characterizing development of the living standards (consumption) of the humans, is maximized. Mathematically, social welfare is represented as

$$W = \int_{T_0}^{\infty} U(c(t), L(t))e^{-\rho(t-T_0)}dt. \tag{12}$$

Here, $U(c(t), L(t))$ is the flow of utility or social well-being, $c(t)$ is the flow of consumption per capita, $L(t)$ is the size of the world population, and ρ is the pure rate of the social time preference. One sets

$$U(c(t), L(t)) = L(t)\ln c(t) \tag{13}$$

and

$$c(t) = \frac{C(t)}{L(t)} \tag{14}$$

where $C(t)$ is the total consumption defined as

$$C(t) = (1-s(t))Q(t). \tag{15}$$

Summarizing, we arrive at the following optimal control problem representing the DICE model:

$$\frac{dK(t)}{dt} = \frac{s(t)(1-b_1\mu(t)^{b_2})A(t)L(t)^{1-\gamma}K(t)^{\gamma}}{1+\theta_1 T^U(t)^{\theta_2}} - \delta_K K(t), \tag{16}$$

$$\frac{dM(t)}{dt} = \alpha(1-\mu(t))\sigma(t)A(t)L(t)^{1-\gamma}K(t)^{\gamma} - \delta_M(M(t)-\tilde{M}), \tag{17}$$

$$\frac{dT^U(t)}{dt} = \frac{1}{R_1}\left(\eta\log_2\left(\frac{M(t)}{\tilde{M}}\right) + O(t) - \lambda T^U(t) - \frac{R_2}{\tau_{12}}\big(T^U(t)-T^L(t)\big)\right), \tag{18}$$

$$\frac{dT^L(t)}{dt} = \frac{1}{\tau_{12}}\big(T^U(t)-T^L(t)\big), \tag{19}$$

$$M(T_0)=M_0, \quad K(T_0)=K_0, \quad T^U(T_0)=T_0^U, \quad T^L(T_0)=T_0^L, \tag{20}$$

$$\mu(t)\in[0,1], \quad s(t)\in[0,1], \tag{21}$$

$$\text{maximize } W = \int_{T_0}^{\infty} e^{-\rho(t-T_0)}L(t)\ln\left(\frac{(1-s(t))(1-b_1\mu(t)^{b_2})A(t)K(t)^{\gamma}L(t)^{1-\gamma}}{\left(1+\theta_1 T^U(t)^{\theta_2}\right)L(t)}\right)dt. \tag{22}$$

3 Exogenous functions, initial conditions and parameters

The DICE model (16)–(22) involves the following exogenous functions describing the dynamics of the model's time-dependent parameters:

$L(t)$, the size of the world population (the world labor force);
$A(t)$, the size of the world technology stock;
$O(t)$, forcing of the exogenous GHGs;
$\sigma(t)$, the carbon intensity of production in the reference case (with the zero controls).

The values of the exogenous functions are determined by the historical data in the historical period. For the future period, they represent admissible scenarios of changes.

In accordance with [1], each of the exogenous functions (except for $O(t)$) is determined by three parameters, the initial value, the growth rate, and the decline in growth, whose values are identified from the historical data. Below, we follow the description of the exogenous functions, given in [1].

For the population size, $L(t)$, one sets:

$$\begin{cases} L(t) = (1+g_L(t))L(t-1), \\ L(T_0) = L_0 \end{cases} \tag{23}$$

where $g_L(t)$ is the population growth rate and L_0 is the population size at the initial time T_0. For the growth rate $g_L(t)$ the following dynamics is assumed:

$$\begin{cases} g_L(t) = g_L(t-1)(1-\delta_L), \\ g_L(T_0) = g_L^0 \end{cases} \tag{24}$$

where δ_L is the rate of decline in the population growth. In the differential form (23) and (24) read:

$$\begin{cases} \dfrac{dL(t)}{dt} = g_L(t)L(t), \\ L(T_0) = L_0, \end{cases} \tag{25}$$

$$\begin{cases} \dfrac{dg_L(t)}{dt} = -\delta_L g_L(t), \\ g_L(T_0) = g_L^0, \end{cases} \tag{26}$$

Solving (25) and (26) with appropriate parameter values, we find:

$$L(t) = 9.3 \cdot e^{(-0.12 \cdot 10^{18} e^{-0.02t})}; \tag{27}$$

Figure 1 shows the graph of $L(t)$.

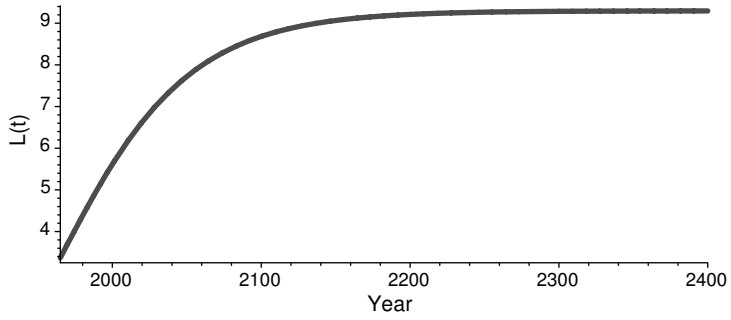

Figure 1:

Similarly, for the size of the technology stock $A(t)$, one sets

$$\begin{cases} A(t) = (1 + g_A(t))A(t-1), \\ A(T_0) = A_0 \end{cases} \tag{28}$$

where $g_A(t)$ is the growth rate described by

$$\begin{cases} g_A(t) = g_A(t-1)(1-\delta_A), \\ g_A(T_0) = g_A^0. \end{cases} \tag{29}$$

The corresponding differential equations are

$$\begin{cases} \dfrac{dA(t)}{dt} = g_A(t)A(t), \\ A(T_0) = A_0, \end{cases} \tag{30}$$

$$\begin{cases} \dfrac{dg_A(t)}{dt} = -\delta_A g_A(t), \\ g_A(T_0) = g_A^0. \end{cases} \tag{31}$$

The sought solution is

$$A(t) = 6.21 \cdot e^{(-0.31 \cdot 10^{10} e^{-0.011t})}. \tag{32}$$

Figure 2 shows the graph of $A(t)$.

The carbon intensity $\sigma(t)$ (the trend in emissions per unit of gross output with the zero controls) is defined by

$$\begin{cases} \sigma(t) = (1 + g_\sigma(t))\sigma(t-1), \\ \sigma(T_0) = \sigma_0 \end{cases} \tag{33}$$

with

$$\begin{cases} g_\sigma(t) = g_\sigma(t-1)(1-\delta_A), \\ g_\sigma(T_0) = g_\sigma^0. \end{cases} \tag{34}$$

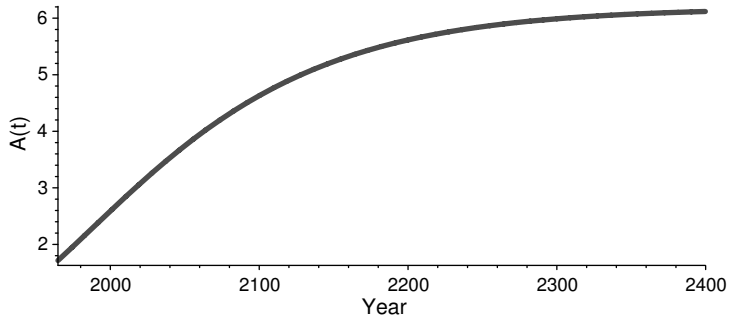

Figure 2:

The corresponding differential equations have the form

$$\begin{cases} \dfrac{d\sigma(t)}{dt} = g_\sigma(t) \cdot \sigma(t), \\ \sigma(T_0) = \sigma_0, \end{cases} \tag{35}$$

$$\begin{cases} \dfrac{dg_\sigma(t)}{dt} = -\delta_A \cdot g_\sigma(t), \\ g_\sigma(T_0) = g_\sigma^0. \end{cases} \tag{36}$$

The sought solution is

$$\sigma(t) = 0.17e^{(0.28 \cdot 10^{10} e^{-0.011t})}. \tag{37}$$

Figure 3 shows the graph of $\sigma(t)$.

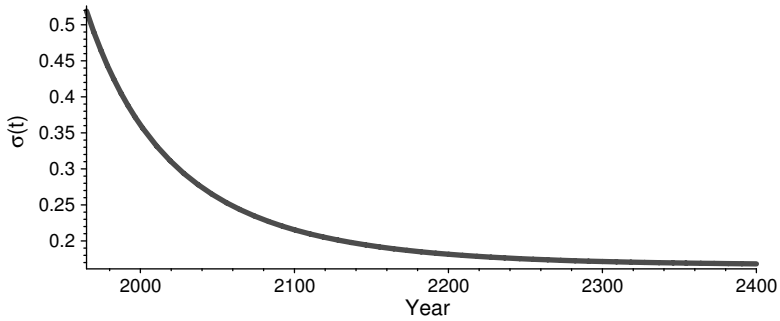

Figure 3:

The exogenous function $O(t)$ is taken in an explicit form[2]:

$$O(t) = \begin{cases} -154.12595 + 0.14544t - 0.000034t^2, & t < 2138, \\ 1.41, & t \geq 2138. \end{cases} \tag{38}$$

Figure 4 shows the graph of $O(t)$.

Along with the exogenous functions, the DICE model (22)–(21) involves several constant parameters whose values are estimated in [1] and given in Table 1. Table 2 gives the initial values for the model's state variables (see [1]).

[2]For more detail see [1, p. 191] ("Appendix: Computer Program for the DICE Model").

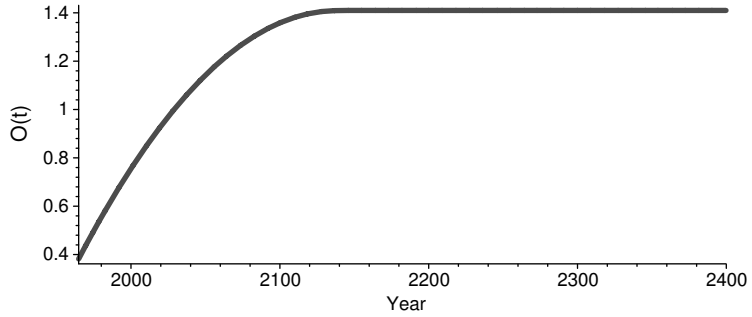

Figure 4:

Table 1:

$\gamma = 0.25$	$\delta_K = 0.1$	$\alpha = 0.64$	$\delta_M = 0.0083$
$b_1 = 0.069$	$b_2 = 2.89$	$\theta_1 = 0.0015$	$\theta_2 = 2$
$\frac{1}{R_1} = 0.226$	$\frac{R_2}{\tau_{12}} = 0.44$	$\frac{1}{\tau_{12}} = 0.02$	$\lambda = 1.41$
$\rho = 0.03$	$\eta = 4.1$	$\delta_L = 0.02$	$g_L^0 = 0.0203$
$\delta_A = 0.011$	$g_A^0 = 0.0141$	$\sigma_0 = 0.519$	

Table 2:

$T_0 = 1965$	year
$K_0 = K(1965) = 16.0$	trillion US$, 1989 prices
$M_0 = M(1965) = 677$	billion tons CO_2 equivalent
$\tilde{M} = 590$	billion tons CO_2 equivalent
$T_0^U = T^U(1965) = 0.2$	degrees C
$T_0^L = T^L(1965) = 0.1$	degrees C
$L_0 = L(1965) = 3.369$	billion persons
$A_0 = A(1965) = 1.72$	
$Q(1965) = 8.519$	trillion US$, 1989 prices

4 Simplification of the DICE model

The DICE-94 model (16)–(22) comprises four differential equations for four state variables, and one utility function. Therefore the model's total dimension is five.

Our primary goal is to carry out an attainability analysis of the DICE model. This type of analysis is especially efficient for 2- and 3-dimensional systems owing to geometrical visuality of 2D and 3D pictures. This fact motivates our preparatory step: the reduction of the dimension of the model. This step is also motivated by limitations in the practical implementation of our analytic technique. Indeed, for complex nonlinear models like the DICE model, any extra dimension may create serious difficulties in the analytic and numerical treatment. Clearly, every simplification of the original model implies some loss in adequacy. Therefore the main requirement for a simplified model is that it should be well adapted to the use of the chosen analytic tool without a considerable loss in adequacy.

For the DICE model, we suggest the following simplification[3]. Let us replace $\Omega(t)$ (11) by

$$\Omega(t) = \frac{1 - b_1\mu(t)^{b_2}}{1 + \theta_1 \left(\frac{M(t)}{\tilde{M}}\right)^{\theta_2}}. \tag{39}$$

Thus, in (11) we replace $T^U(t)$ by $M(t)/\tilde{M}$. i.e., we approximate the temperature change by the change in the atmospheric CO_2 level. This approximation reduces the model's dimension to three (including two state variables and one utility index). Indeed, using (39) instead of (11), we exclude the climate equations (18) and (19), and get the following simplified model:

$$\frac{dK(t)}{dt} = \frac{s(t)(1 - b_1\mu(t)^{b_2})A(t)L(t)^{1-\gamma}K(t)^{\gamma}}{1 + \theta_1 \left(\frac{M(t)}{\tilde{M}}\right)^{\theta_2}} - \delta_K K(t), \tag{40}$$

$$\frac{dM(t)}{dt} = \alpha(1 - \mu(t))\sigma(t)A(t)L(t)^{1-\gamma}K(t)^{\gamma} - \delta_M(M(t) - \tilde{M}), \tag{41}$$

$$M(T_0) = M_0, \quad K(T_0) = K_0, \tag{42}$$

$$0 \le \mu(t) \le 1, \quad 0 \le s(s) \le 1, \tag{43}$$

$$\text{maximize} \quad W = \int_{T_0}^{\infty} e^{-\rho(t-T_0)} L(t) \ln\left(\frac{(1 - s(t))(1 - b_1\mu(t)^{b_2})A(t)K(t)^{\gamma}L(t)^{1-\gamma}}{\left(1 + \theta_1\left(\frac{M(t)}{\tilde{M}}\right)^{\theta_2}\right)L(t)}\right)dt. \tag{44}$$

5 Comparison of the models

The simplified DICE model comprises two state equations, (40) and (41), and one utility index, (44). This gives us the possibility to show the model's states in 2D- or 3D-plots.

Prior to go to our attainability analysis, we address, in brief, the following question: to which extent the trajectories of a the simplified model (40)–(44) agree with the trajectories of the original model (16)–(22)? Our numerical simulations show that the trajectories of the simplified model and those of the original model lie very close to each other; a slight difference appears after an approximately 300-years period. Figure 5 shows the trajectories of the original model and those of the simplified model with $\mu(t) = 0.2$ and $s(t) = 0.2$.

In our further simulations, we take into consideration the utilities (44) and (22) and compare the optimal solutions for the original optimization problem, (16)–(21), and the simplified one, (40)–(42). Figure 6 shows the optimal controls $\mu(t)$ and $s(t)$, and Figure 7 the optimal trajectories for the original and simplified DICE models[4].

We see slight deviations in the controls (almost none in $s(t)$) and in the trajectories. The registration of slight variations in the simulation results allows us to conclude that the simplified model (40)–(44), compared to the original model (16)–(22), does not lose much in adequacy. Therefore, the simplified model is appropriate for studying the geometrical properties of the DICE trajectories.

[3]The simplification was suggested by Brian O'Neil and Michael Obersteiner.

[4]Nordhaus [1] presents a solution for the original DICE model, which is derived using the GAMS software package. We also use the GAMS tool to find a solution for the simplified DICE model.

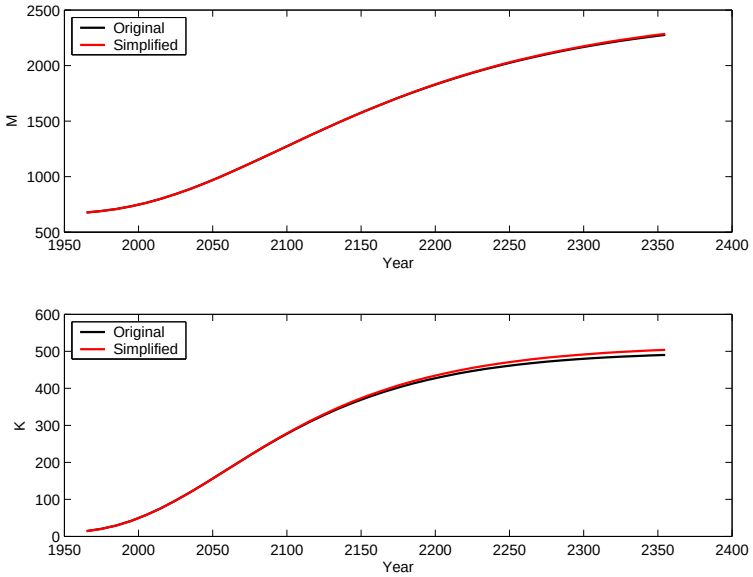

Figure 5:

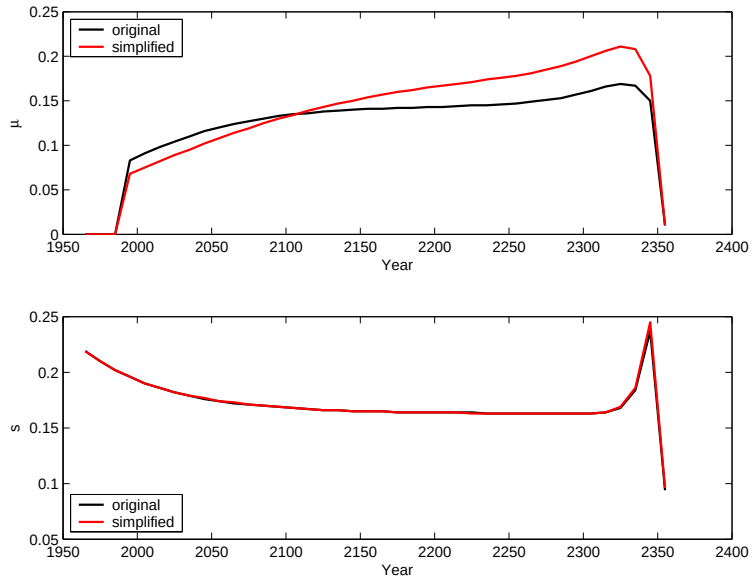

Figure 6:

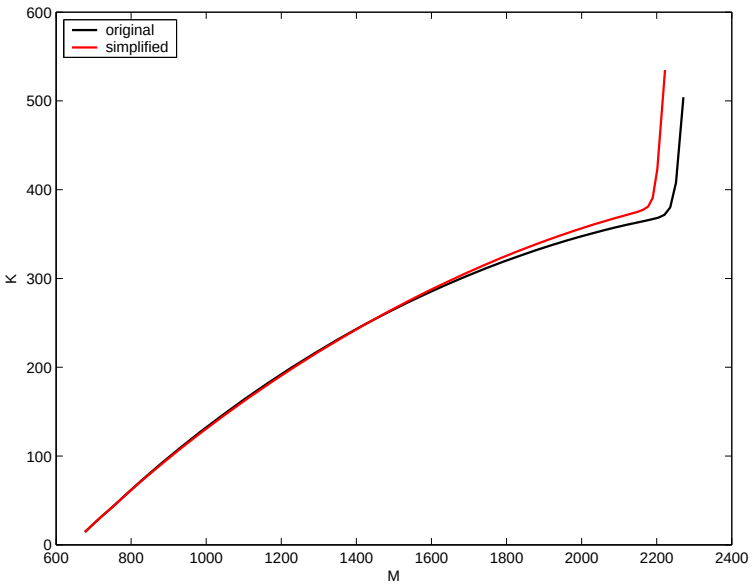

Figure 7:

6 Model adjustment

Now we compare the models in a different way. Recall that in [1] the trajectories of the DICE model are constructed using the GAMS software package known as a solver to finite-dimensional optimization problems. However the original DICE optimization problem (16)–(21) (as well as the simplified one, (40)–(44)) is infinite-dimensional since part of its constraints are given in the form of continuous-time differential equations. Therefore it is not surprizing that [1] introduces a descrete-time approximation to the continuous-time dynamical system.

A simple illustration for the descrete-time approximation approach is as follows. Assume we deal with a continuous-time optimization problem

$$\begin{cases} \dfrac{dx(t)}{dt} = f(x(t), u(t)), \quad x(0) = x_0, \quad u(t) \in U, \quad t \in [0, T], \\ \qquad \text{maximize } J(x, u). \end{cases} \tag{45}$$

We fix a time step Δ and introduce a discrete-time approximation to (45):

$$\begin{cases} x_{i+1} = x_i + \Delta \cdot f(x_i, u_i), \quad x_1 = x_0, \quad u_i \in U, \quad i = 1, \dots, n, \\ \qquad \text{maximize } J(x_1, x_2, \dots, x_n, u_1, u_2, \dots, u_n). \end{cases} \tag{46}$$

We see that (46) is a finite-dimensional optimization problem, for which standard solvers including the GAMS package can be applied. Note that a solution of (46) is an approximation to a solution of (45). However, under appropriate assumptions one can prove that the approximation error is arbirtarily small if the time step Δ is sufficiently small.

In [1], the discrete-time approximation to the original continuous-time DICE model (16)–(22) is constructed with the 10-years time step, and the parameter values given in Table 1 (see Section 3) are identified for that approximate discrete-time model. Note that the discrete-time model produces approximate states at discrete points in time. Our goal is however to explore the DICE model with continuous time. Namely, we want to make use of analytic tools of optimal control theory dealing with continuos-time dynamical systems; the DICE problems (16)–(22) and (40)–(44) fall entirely into the scope of that

theory (see [2]). Therefore, prior to starting our control-theoretic analysis, we will compare simulation results for the original continuous-time DICE model and its discrete-time approximation.

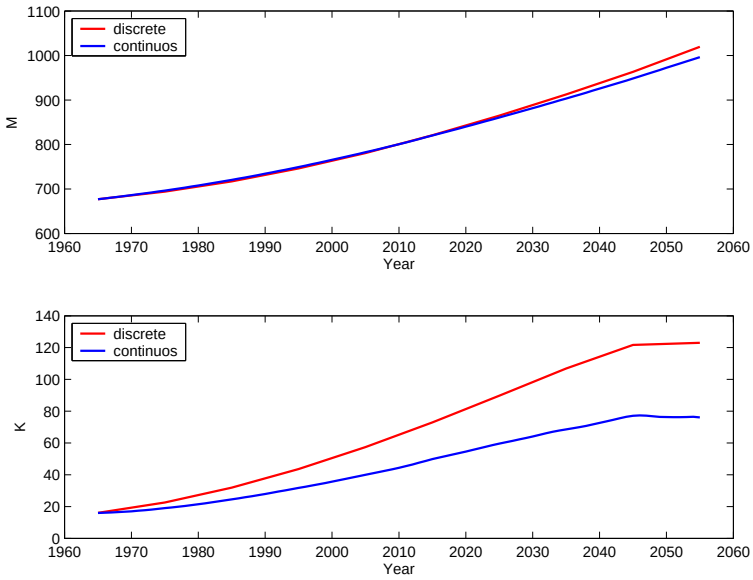

Figure 8:

Figure 8 shows the trajectories of the discrete-time and continuous-time DICE models, driven by the same controls. We see a significant discrepancy in $K(t)$. For this reason,

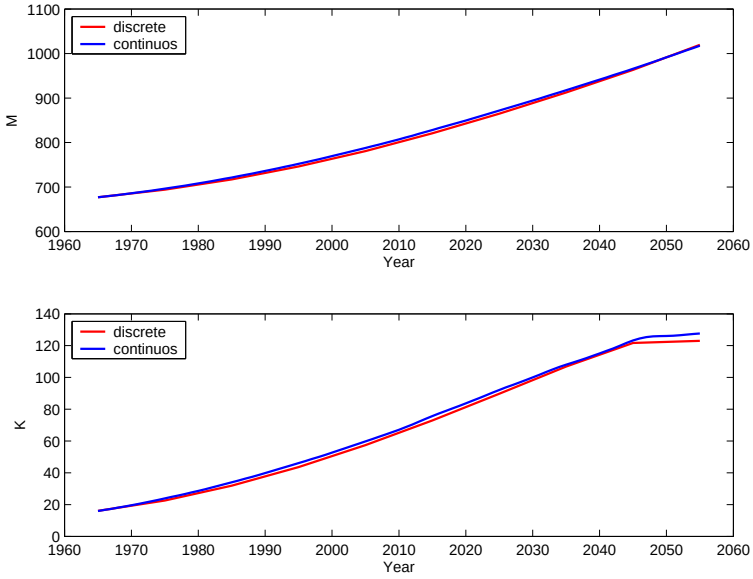

Figure 9:

we recalibrate the continuous-time model so as to make its trajectories consistent with those of the discrete-time model. We adjust the values for δ_M and δ_K as shown in Table 3 and obtain the trajectories depicted in Figure 9. We see that now the trajectories of the discrete-time and continuous-time models practically coincide. We conclude that the simplified continuous-time DICE model (40)–(44) imitates the discrete-time DICE trajectories given in [1] with a good accuracy. In other words, the simplified continuous-time

Table 3:

	Original value	Adjusted value
δ_M	0.0083	0.0095
δ_K	0.1	0.066

DICE model (40)–(44) with the parameter values presented in Tables 1–3 is nearly as adequate as the original discrete-time DICE model constructed in [1].

7 Attainability domains: an introduction

In this section, we give a short overview of some concepts and results of optimal control theory (see [2]).

Let us consider a dynamical system described by a differential equation with a control parameter:

$$\begin{cases} \dfrac{dx(t)}{dt} = f(t, x(t), u(t)), \quad u(t) \in U, \quad t \in [t_0, T], \\ x(t_0) = x_0. \end{cases} \tag{47}$$

Here, $x(t)$ is a finite-dimensional vector representing the system's state at time t; $u(t)$ is the value of the (finite-dimensional) control parameter at time t; U is a set characterizing the controller's resources; t_0 is the initial time; and $T > t_0$ is a given time horizon. An admissible control is understood as an arbitrary function of time, $u(t)$, taking values in U (here we omit additional technical constraints normally imposed on the admissible controls in order to guarantee the solvability of the differential equation (47)).

Take an arbitrary admissible control $u_1(t)$ and substitute it as $u(t)$ in (47). This turns (47) into a particular differential equation. Solving that differential equation over the time interval $[t_0, T]$, we find the system's state at time T: $x_1(T)$. We can say that the admissible control $u_1(t)$ brings the system from the initial state x_0 to state $x_1(T)$ at time T (see Figure 10). Now let us take another admissible control, $u_2(t)$, and find the state $x_2(T)$,

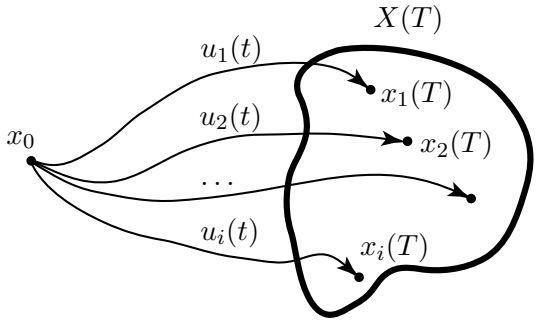

Figure 10:

to which $u_2(t)$ brings the system at time T. Let us repeat this process many times with different admissible controls. If we run through all admissible controls (which is a merely imaginary process since the space of the admissible controls is infinite-dimensional), we obtain a set of the system's states reachable at time T: $X(T)$. The latter set is called the attainability domain of the dynamical control system (47) at time T. More formally, the

attainability domain of the dynamical control system (47) at time T is defined to be the set $X(T)$ of the final points $x(T)$ of all the solutions to system (47), corresponding to all admissible controls $u(t)$.

As noted above, it is impossible to construct $X(t)$ directly, i.e., through going through all admissible controls and solving the infinite-dimensional family of differential equations. However, optimal control theory suggests powerful indirect methods for constructing the attainability domains.

We use the Pontryagin maximum principle (see [2]) to describe the boundary of the attainability domains for the dynamical system defining the simplified DICE model. Our method employs the following property (see, e.g., [3]): an admissible control $u_*(t)$ that brings the control system (47) from the given initial state x_0 to a point $x_*(T)$ on the boundary of the attainability domain $X(T)$ is necessarily optimal with respect to a certain (fictitious) performance index and consequently satisfies – together with the corresponding trajectory $x_*(t)$ – a necessary optimality condition: the Pontryagin maximum principle. The latter claims that there exists a nonzero function of time, $\psi_*(t)$, (called the adjoint variable) such that

(i) $x_*(t)$ and $\psi_*(t)$ solve the following system of interconnected differential equations:

$$\begin{cases} \dfrac{dx(t)}{dt} = \dfrac{\partial \mathcal{H}(t, x(t), \psi(t), u_*(t))}{\partial \psi}, & t \in [t_0, T], \\ \dfrac{d\psi(t)}{dt} = -\dfrac{\partial \mathcal{H}(t, x(t), \psi(t), u_*(t))}{\partial x}, \\ x(t_0) = x_0, \\ x(T) = x_1, \end{cases} \tag{48}$$

and

(ii) for each time t the maximum condition holds:

$$H(t, x_*(t), \psi_*(t)) = \mathcal{H}(t, x_*(t), \psi_*(t), u_*(t)). \tag{49}$$

Here, $\mathcal{H}(t, x, \psi, u)$ is the Hamilton-Pontryagin function defined by

$$\mathcal{H}(t, x, \psi, u) = \langle \psi, f(t, x, u) \rangle \tag{50}$$

($\langle \cdot, \cdot \rangle$ denotes the inner product in the system's state space), and $H(t, x, \psi)$ is the Hamiltonian defined by

$$H(t, x, \psi) = \max_{u \in U} \mathcal{H}(t, x, \psi, u). \tag{51}$$

In the case where the Hamiltonian is differentiable in x and in ψ ($\psi \neq 0$), one can rewrite (48) in an equivalent form excluding $u(t)$:

$$\begin{cases} \dfrac{dx(t)}{dt} = \dfrac{\partial c(F(t, x(t)), \psi(t))}{\partial \psi}, & t \in [t_0, T], \\ \dfrac{d\psi(t)}{dt} = -\dfrac{\partial c(F(t, x(t)), \psi(t))}{\partial x}, \\ x(t_0) = x_0, \\ x(T) = x_1; \end{cases} \tag{52}$$

here

$$F(t, x) = \{ f(t, x, u) \mid u \in U \}, \tag{53}$$

$$c(F, \psi) = \max_{f \in F} \langle f, \psi \rangle \tag{54}$$

($F(t,x)$ is known as the system's vectogram at point (t,x), and $c(F,\psi)$ as the support function of $F(t,x)$)). In this case, for every point x_1 on the boundary of the attainability domain $X(T)$, there exists a solution $(x(t),\psi(t))$ of (52) with $\psi(t_0)\neq 0$.

Now consider the differential equation similar to (52), in which, however, the location x_1 of $x(T)$ is not fixed and the location of $\psi(0)$ is viewed as a nonzero parameter p:

$$\begin{cases} \dfrac{dx(t)}{dt} = \dfrac{\partial c(F(t,x(t)),\psi(t))}{\partial \psi}, \quad t\in[t_0,T], \\ \dfrac{d\psi(t)}{dt} = -\dfrac{\partial c(F(t,x(t)),\psi(t))}{\partial x}, \\ x(t_0)=x_0, \\ \psi(t_0)=p, \quad p\neq 0. \end{cases} \tag{55}$$

It is known that if system (47) is linear, the Pontryagin maximum principle serves as both a necessary condition and a sufficient condition for bringing the system to the boundary of the attainability domain. In this situation, the final point $x(T)$ of the x-component of the solution $(x(t),\psi(t))$ of (55) encircles precisely the boundary of the attainability domain $X(T)$ as p runs through all nonzero states. Moreover, owing to the linearity of the equation for the adjoint variable in (55), p is allowed to run through the unit sphere only.

In the case where system (47) is nonlinear, the point $x(T)$, with p running through the unit sphere, encircles the boundary of the attainability domain $X(T)$ and, possibly, goes also into the interior of $X(T)$ along some "extra" curve. Although the "extra" curve may, in principle, introduce some fuzziness in the interpretation of the result, practically one can easily separate the "extra" curve from the boundary of $X(T)$.

As our next step, we take into consideration a utility index $J(x,u)$ to be maximized over the trajectories and the controls of system (56). Thus, we consider the optimal control problem

$$\begin{cases} \dfrac{dx(t)}{dt} = f(t,x(t),u(t)), \quad u(t)\in U, \quad t\in[t_0,T], \\ x(t_0)=x_0, \\ \qquad \text{maximize } J(x,u). \end{cases} \tag{56}$$

Bringing our argument closer to our simplified DICE model, we assume that the state space of system (47) (see also (56)) is two-dimensional, therefore we can view the attainability domain $X(T)$ as a domain in the horizontal plane. Take an arbitrary point x_1 in $X(T)$ and add one more constraint to problem (47):

$$x(T)=x_1. \tag{57}$$

In the new optimal control problem, (56), (57), it is required to bring the system from the initial point x_0 to the prescribed point x_1 in $X(T)$ at time T, with the maximum value of the utility, $J(x,u)$. Assume we solve this problem. Let us place the maximum value of $J(x,u)$ on the vertical axis above the point x_1 in the three-dimensional space (see Figure 11). Repeating this procedure for every point $x_1=x(T)$ in $X(T)$, we construct a surface, S, in the three-dimensional space. Each point $(x(T),J)$ on S shows us the maximum value of the utility $J(x,u)$, which is achievable by the system under the condition that it is brought to state $x(T)$ at time T. The highest point on S corresponds to the solution of problem (56).

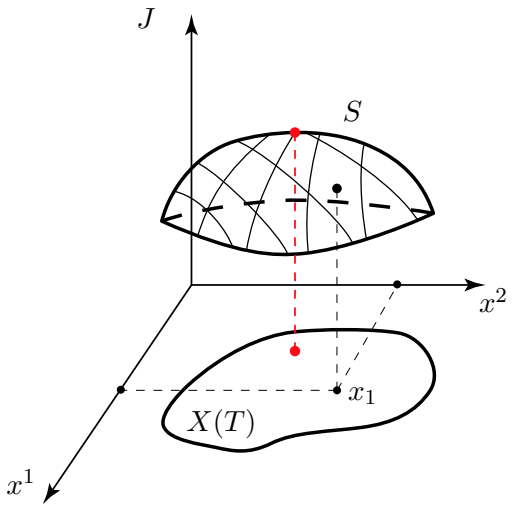

Figure 11:

Surface S, which we will call the utility surface, gives us a rich information on the control system. Looking at it, we simultaneously observe all the system's states reachable at the final time T, which allows us to identify sets of the final states that, not being fully optimal, are appropriate (suboptimal) in terms of the utility. Having identified such sets we receive a freedom of choosing within a variety of suboptimal control modes.

8 Attainability analysis of the DICE model

To construct the attainability domain at time T for the simplified DICE system (40)–(41), we use the numerical integration of equation (55) (specified according to the form of the system). All calculations were performed using the MAPLE software package.

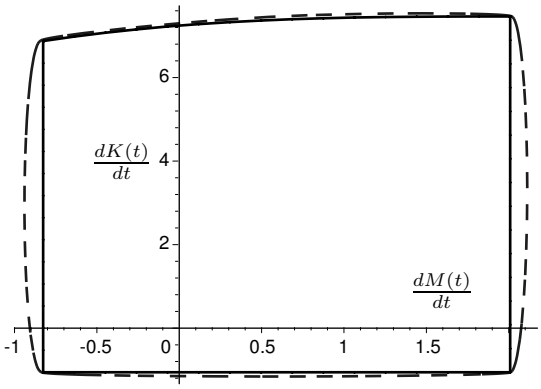

Figure 12:

First, we construct the vectogram (53) for the DICE equations (40)–(41). We find that this vectogram (being a set on the plane) is not strictly convex (Figure 12 shows the simplified DICE system's vectogram at the initial state T_0, K_0, M_0). This observation implies that the Hamiltonian (see (51)) of the DICE system (40)–(41) is not differentiable at some points. The nondifferentiability of the Hamiltonian may lead to technical difficulties in the integration of system (55). Moreover, the nondifferentiability of the Hamiltonian implies that the controls bringing the system to the boundary of the attainability domain may be singular, i.e., non-identifiable through the Pontryagin maximum principle, on some time

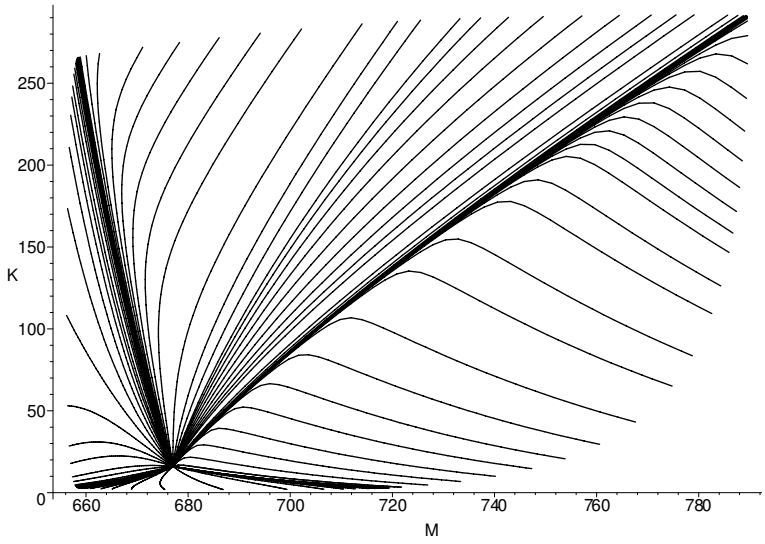

Figure 13:

intervals. In order to eliminate singular controls, we slightly perturb (smooth out) the system's vectogram so that the perturbed vectogram becomes strictly convex. Although the perturbed vectogram corresponds to a perturbed DICE system, one can make the perturbation in the system dynamics arbitrarily small by letting a special parameter controlling the perturbation of the vectogram go to zero. Figure 13 shows the trajectories of the coupled system (55) (constructed for the DICE dynamics (40)–(41)) with different initial values p for the adjoint variable $\psi(t)$ (located on the unit sphere). The final points of these trajectories lie on the boundary of the attainability domain for the perturbed DICE system. Figure 14 shows the controls that bring the perturbed DICE system from

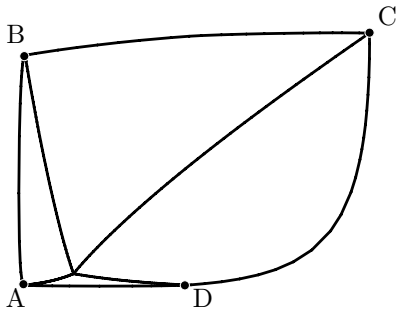

$$A:\ \mu=1,\ s=0 \quad \widehat{AB}:\ \mu=1,\ s=\text{const}\in[0,1]$$
$$B:\ \mu=1,\ s=1 \quad \widehat{BC}:\ \mu=\text{const}\in[0,1],\ s=1$$
$$C:\ \mu=0,\ s=1 \quad \widehat{CD}:\ \mu=0,\ s=\begin{cases}1,\ t<t^*,\ t^*\in[0,T]\\ 0,\ t\geq t^*\end{cases}$$
$$D:\ \mu=0,\ s=0 \quad \widehat{DE}:\ \mu=\text{const}\in[0,1],\ s=0$$

Figure 14:

the initial point to the boundary of its attainability domain, and Figure 15 shows the trajectories of the non-perturbed DICE system (40)–(41), driven by those controls. We see that the trajectories of the non-perturbed DICE system (Figure 15) and those of the perturbed DICE system (Figure 13) differ not essentially.

The curve drown through the endpoints of the trajectories of the perturbed DICE system (Figures 13) gives us the boundary of its attainability domain; the latter curve serves as an approximation to the boundary of the attainability domain for the non-perturbed DICE system. The curve drown through the endpoints of the trajectories of the non-perturbed DICE system (Figures 15) gives us another approximation to the boundary of the attainability domain for the non-perturbed DICE system. These two approximating curves are shown in Figure 16. We see that the approximating curves lie very close to each other provided the vectogram perturbation parameter is sufficiently small.

This numerical test allows us to conclude the following. The boundary of the attain-

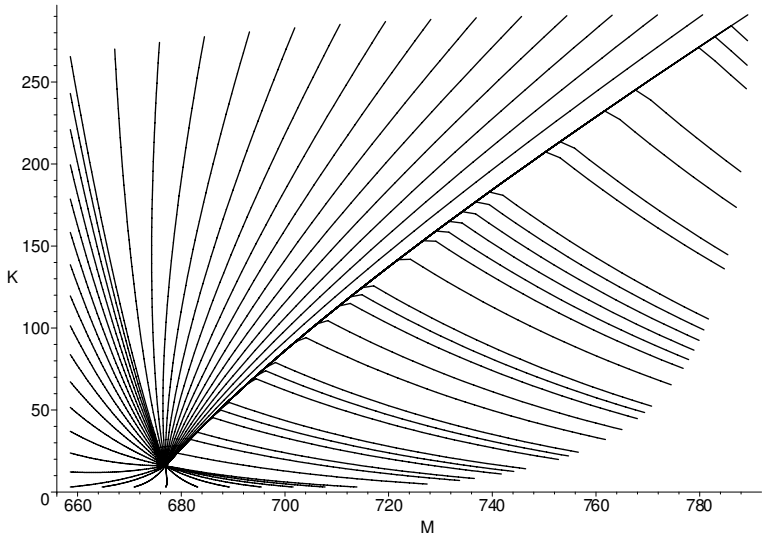

Figure 15:

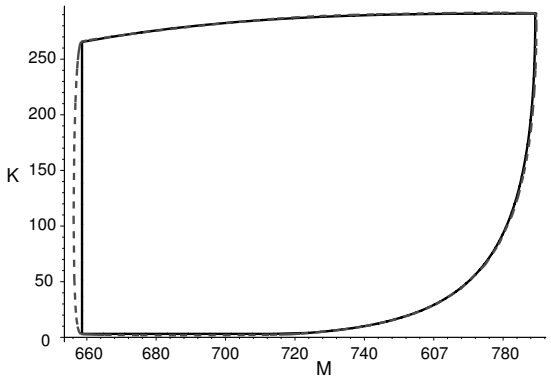

Figure 16:

ability domain for the non-perturbed DICE system (40)–(42) is quite accurately approximated by the curve that connects the endpoints of the system's trajectories driven by the extremal controls for the perturbed DICE system (see Figure 14) – as the initial point for the adjoint variable, p, runs through the unit sphere on the plane.

Figure 17 shows the attainability domain for the DICE system (40)–(42) at the year 2005. Figure 18 shows the system's attainability domains at several selected years in the future.

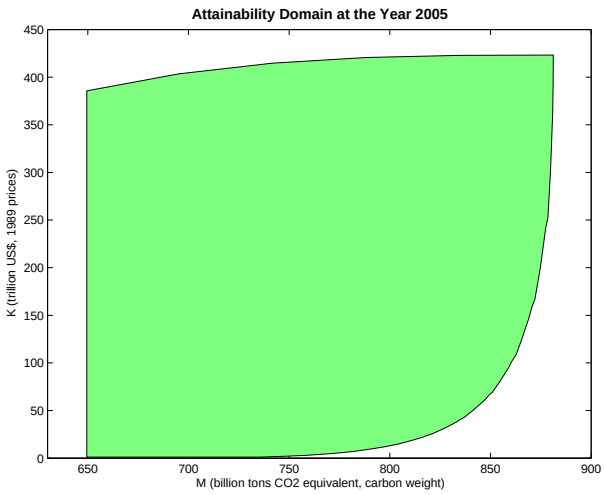

Figure 17:

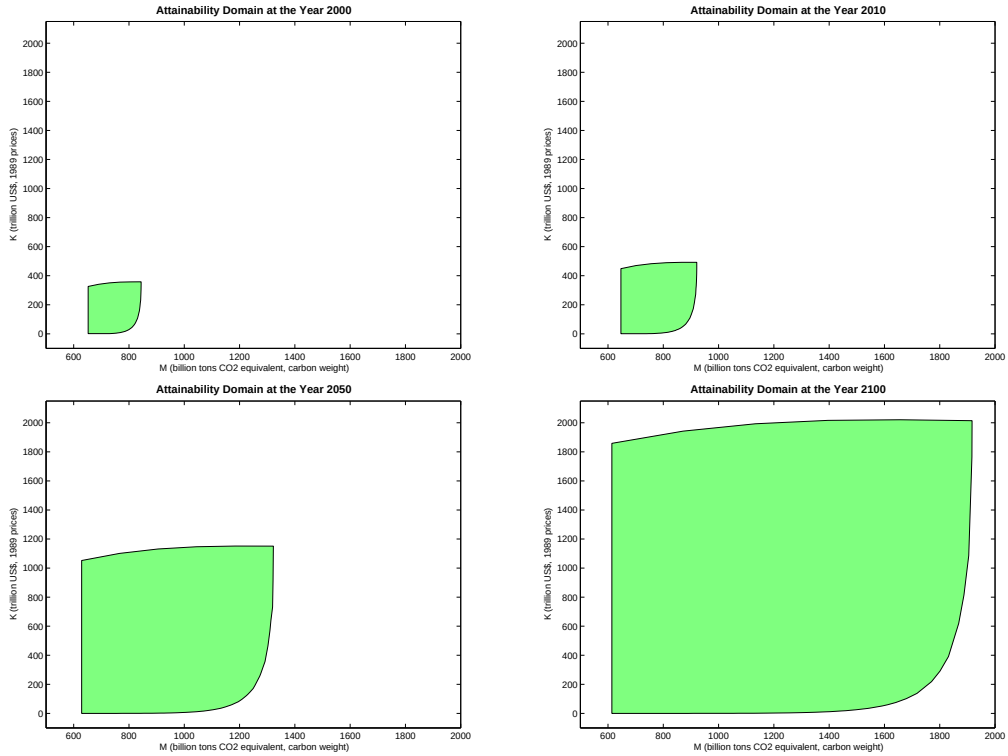

Figure 18:

The next stage in our numerical analysis[5] is the construction of the utility surface over the attainability domain for the DICE system (40)–(42). Recall that the procedure for the construction of the utility surface (see Section 7) recommends us to take points in the attainability domain and find the controls bringing the system to these points. If several controls bring the system to the same point, we should choose those of them, which maximize the utility. In other words, for each point in the attainability domain, considered as a prescribed final point of the system, we should solve the optimal control problem with the fixed initial and final points.

We, however, use a simpler algorithm. We restrict ourselves to controls $\mu(t)$, $s(t)$ taking constant values $\mu_1, \mu_2, \mu_3 \in [0,1]$, $s_1, s_2, s_3 \in [0,1]$, on the intervals $[T_0, t_1)$, $[t_1, t_2)$, $[t_2, T]$, respectively, with some switching times $t_1, t_2 \in [T_0, T]$, $t_2 \geq t_1$ (see Figure 19). Let us call such controls two-switch controls.

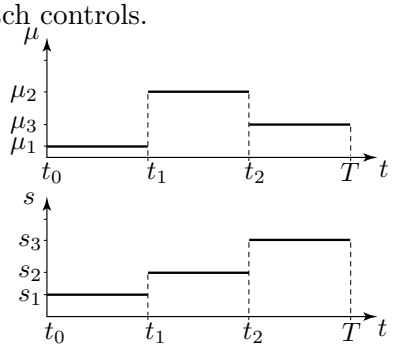

Figure 19:

For each two-switch control $\mu(t)$, $s(t)$ we simulate the trajectory of the DICE system (40)–(42), find the corresponding value of the utility, and store that value together with

[5] We used the MATLAB system.

the final point of the trajectory (which clearly lies in the system's attainability domain). In this manner, we cover the entire attainability domain, and for each point in it find the value of the utility. Figure 20 shows the surface formed by these utility values placed on the vertical axis above the corresponding points in the attainability domain. Let us call this surface the approximate utility surface.

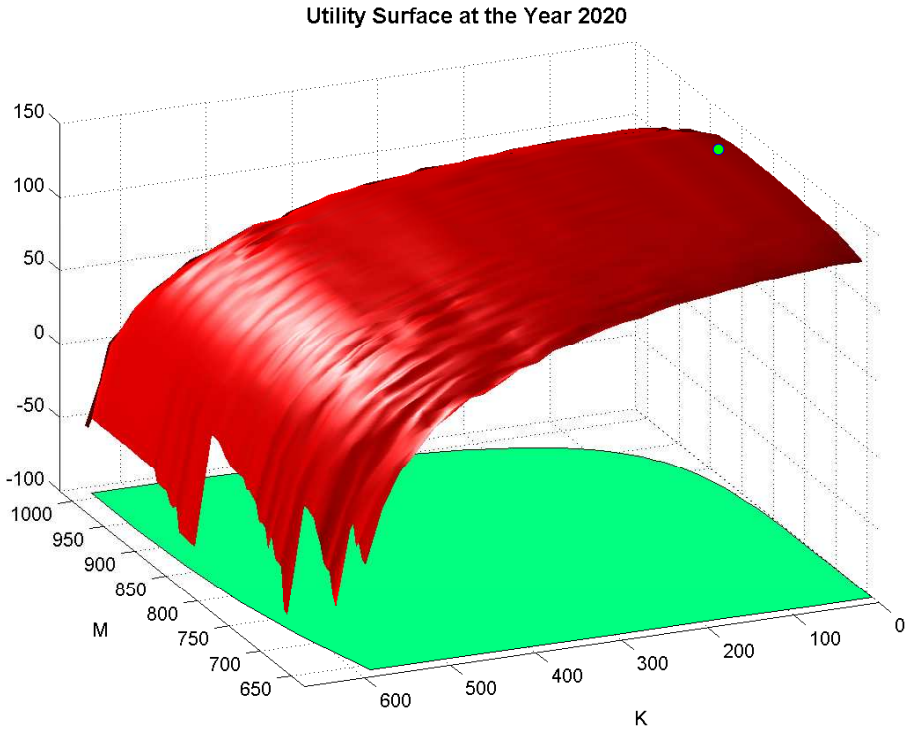

Figure 20:

We claim that the approximate utility surface approximates the utility surface defined in Section 7 (see Figure 11) with a good accuracy.

We explain this as follows.

First, it is proved numerically that the DICE system (40)–(42) reaches any interior point in its attainability domain using the two-switch controls.

In our second argument, we refer to the white dot in Figure 20, which shows the optimal point in the DICE model (at this point the DICE model (40)–(44) reaches its maximum utility). The optimal point was found using a direct optimization method. However, we see that the optimal point lies on the top of the approximate utility surface; in other words, having the approximate utility surface, we can identify the optimal solution in the DICE model (40)–(44).

Our third argument is qualitative. Figure 20 shows that the approximate utility surface is almost flat in quite a large neighborhood of its highest point (i.e., the optimal point in the DICE model). If we assume that there are controls that provide much greater values to the utility than the two-switch controls, then the exact utility surface should lie considerably higher than the approximate utility surface (see Figure 20). However, this is practically impossible – at least in quite a large neighborhood of the optimal point – because the optimal point lies on the approximate utility surface and the latter is almost flat.

In what follows, we represent the utility surface as a map showing us the attainability domain whose points are colored according to the hight of the utility surface at these points. Figure 21 depicts the utility surface given in Figure 20, visualized in this manner.

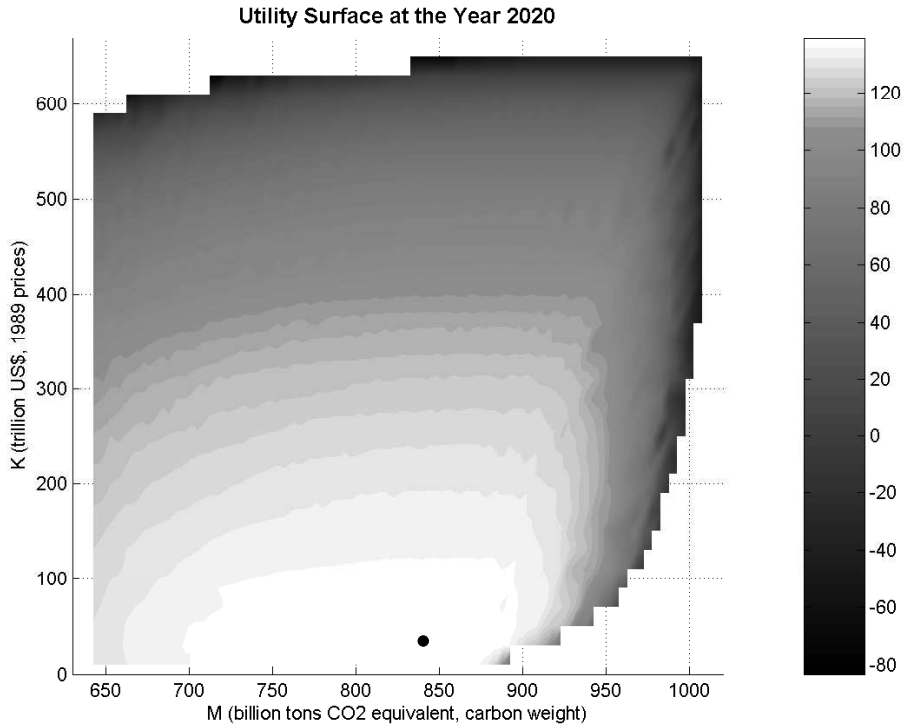

Figure 21:

The gray scale varying from black to white shows the increasing hight of the utility surface. The black color corresponds to the lowest value of the utility and the white color to its highest value. The black dot shows the optimal point, at which the utility reaches its maximum value. A large neighborhood of the optimal point is colored white, implying that in this neighborhood the utility is very close to its maximum value. In practical terms, any point within this neighborhood can be viewed as an optimal one. In geometrical terms, the utility surface is practically "flat" in quite a large neighborhood of the optimal point. This is clearly seen in Figure 22 showing the utility surfaces for the years 2005, 2020, 2050, and 2100. In this figure, the color scale is given in percents to the maximum hight of the utility surface.

In Figure 22 the white zone comprises all the points, at which the utility takes values not less than 98% of its maximum value (the latter is reached at the point marked by the circle dot). We see that for each year the white zone covers a considerable part of the attainability domain, and its relative area grows over time; in other words the utility surface becomes "more and more flat" as the time horizon grows.

Note that the phenomenon of the "increasing flatness" is typical for dynamic optimization models with a discount factor in the utility. In this context, it is important that in the DICE system a "flat" utility surface appears at extremely short time horizons, at which the discount factor does not yet play a principal role, and is stably kept over the longer time horizons. In other words, the "flatness" of a considerable part of the utility surface, around the optimal point on it, is an immanent feature of the DICE system.

Furthermore, as Figure 22 shows, the "flat" white zone is asymmetric; it is relatively short along the K axis and quite long along the M axis. This observation reveals the fact that the DICE system responds differently to variations of the controls $s(t)$ and $\mu(t)$. A sensitivity analysis of the dynamics of the DICE system (40)–(41) allows us to understand the nature of the asymmetry. We find that moderate variations in $\mu(t)$ may significantly

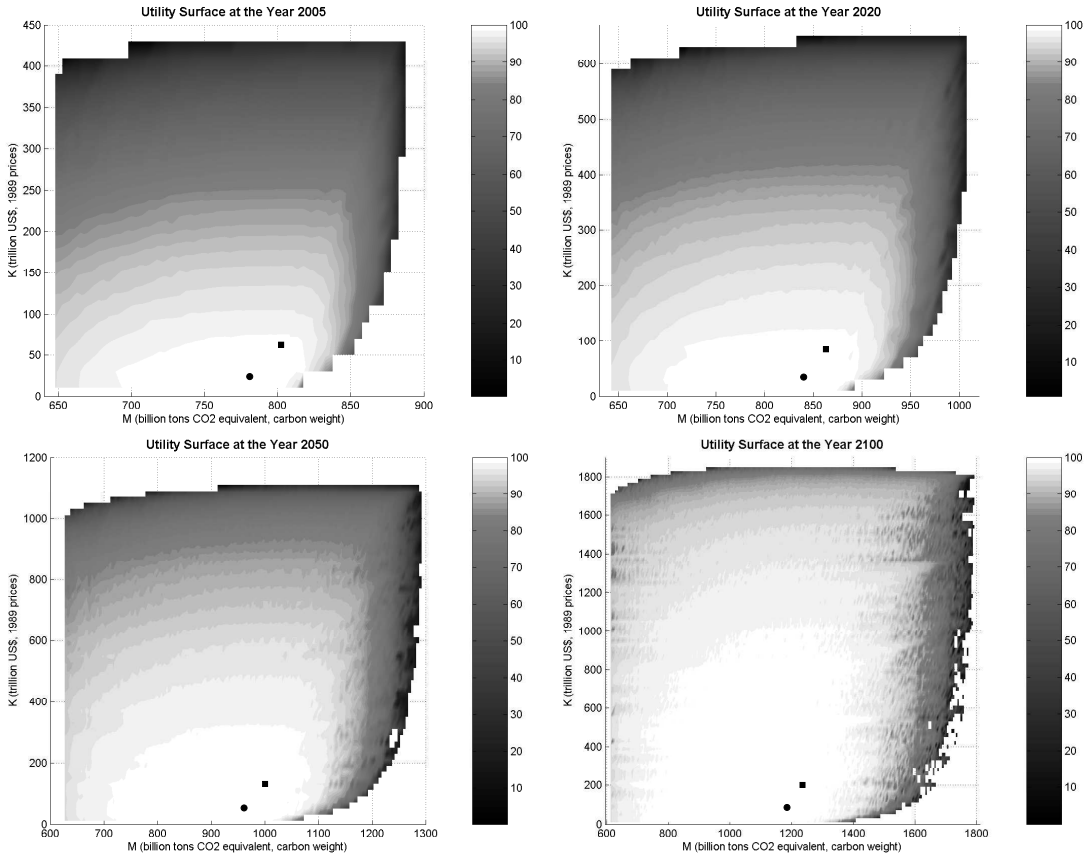

Figure 22:

change the CO_2-concentration (the state variable M) without a serious effect on the size of capital (the state variable K). On the other hand, moderate variations in control $s(t)$ representing the saving rate may significantly change both state variables, M and K.

In Figure 22 the black square dots mark the points called here the Nordhaus points; these are the states, to which the DICE system arrives (at the corresponding times) under the action of the controls $\mu(t)$ and $s(t)$ found by Nordhaus [1] as a solution to the DICE optimization model. The Nordhaus points differ notably from the circle dots marking the optimal points for the corresponding time horizons (note that the Nordhaus points lie in the white zones of "flatness"). This is not surprising since the DICE model is originally formulated as an optimization problem with the infinite time horizon (see (16)–(22), (40)–(44)); accordingly, the Nordhaus points lie on the DICE trajectory that is optimal over the infinite time interval, whereas the points marked with the circle dots lie on the trajectories that are optimal over the finite time intervals. More accurately, each circle dot marks the final point of the trajectory, at which the utility is maximized for a particular finite time horizon. These finite-horizon trajectories are obviously differ pairwise and each of them differs from the DICE trajectory that is optimal for the infinite horizon. Therefore, the fact that the circle dots (the optimal points for the finite time horizons) and square dots (the Nordhaus points) do not coincide is absolutely natural. It simply says that maximizing welfare up to, say, the year 2050, is not the same as maximizing it with an open time horizon.

Our analysis of the simplified DICE system shows that attainability domains and utility surfaces can provide useful information for comparing control strategies. Note that

based on the data used to construct the utility surface, other informative surfaces, such as the GWP surface (1), or per capita consumption surface (14)), can be built up (see Figure 23).

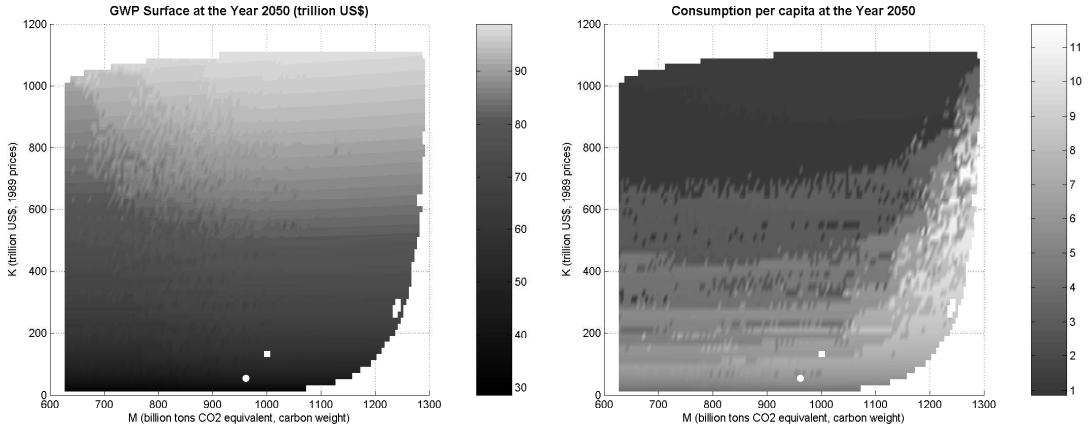

Figure 23:

9 Conclusions

In this paper, we study a simplified the DICE model (see (40)–(44) and Table 1–2). We adjust its parameters (Table 3) so that the trajectories of the original DICE-94 model (see [1]) are reproduced with a good accuracy. For the simplified model, we construct the attainability domains (Figure 18) and the utility surfaces (Figure 22). Based on a comparison of the models (Section 5), we assert that several key properties of the simplified model hold for the original model. An important result of our attainability analysis is that for each time horizon, the utility surface of the DICE system (Figure 22) is practically "flat" in a large neighborhood of its highest (optimal) point. Therefore, for any given finite time horizon, there is a variety of suboptimal controls that steer the system to different final states with practically no loss in the utility, compared to its optimal value. In other words, there is a variety of strategies to control CO_2-emission, which can be viewed as "practically optimal" in terms of social welfare. Based on that, we conclude that when identifying a "fully" optimal control strategy it is desirable to complement social welfare with other optimality criteria (visualized as surfaces, some of which are shown in Figure 23).

One of such criteria could be the concentration of CO_2. In this context it is interesting to note that the "flat" zone on the utility surface (see Figure 22) is oblong in the direction of the CO_2 concentration axis, which is a consequence of a high sensitivity of the system's CO_2 concentration state variable with respect to variations in the rate of emission reduction. One can find such variations of the optimal emission reduction rate that the loss in the utility is neglectable, whereas the value of the concentration of CO_2 decreases significantly.

Many questions related to the DICE model are still remaining open. The question of the model's sensitivity – including the sensitivity of the utility surface to changes in the model's parameters – is among them.

References

[1] *Nordhaus, W.D.*, Managing the Global Commons. The Economics of Climate Change, MIT Press, 1994.

[2] *Pontryagin, L.S., Boltyanskii, V.G., Gamkrelidze, R.V., and Mishchenko, E.F.*, Mathematical Theory of Optimal Processes, Interscience Publishers, John Wiley & Sons, New York, 1962.

[3] *Lee, E.B., Markus, L.*, Foundations of Optimal Control Theory, John Wiley & Sons, New York, 1967.

[4] *Kurzhanskii, A.B., Valyi, I.*, Ellipsoidal Calculus for Estimation and Control, Birkhauser, Boston, 1997.

[5] *Chernousko, F.L.*, State Estimation of Dynamical Systems: Ellipsoidal Approach, Nauka, Moscow, 1988.

[6] *Nordhaus, W.D., Boyer, J.*, Warming the World — Economic Models of Global Warming, MIT Press, 2001.